ACS APPLIED MATERIALS & INTERFACES

Research Article

www.acsami.org

Additive-Free Synthesis of In_2O_3 Cubes Embedded into Graphene Sheets and Their Enhanced NO_2 Sensing Performance at Room Temperature

Wei Yang,[†,‡] Peng Wan,[§] Xiaodong Zhou,[‡] Jiming Hu,[‡] Yafeng Guan,[†] and Liang Feng*[,†]

[†]Key Lab of Separation Science for Analytical Chemistry, Dalian Institute of Chemical Physics, Chinese Academy of Sciences, Dalian 116023, P.R. China

[‡]Key Lab of Analytical Chemistry for Biology and Medicine (Ministry of Education), College of Chemistry and Molecular Sciences, Wuhan University, Wuhan 430072, P.R. China

[§]Faculty of Chemical, Environmental, and Biological Science and Technology, Dalian University of Technology, Dalian 116024, P.R. China

Supporting Information

ABSTRACT: In this report, we developed an additive-free synthesis of In_2O_3 cubes embedded into graphene networks with InN nanowires (InN-NWs) and graphene oxide (GO) as precursors by a facile one-step microwave-assisted hydrothermal method. In absence of GO, the InN-NWs maintained their chemical composition and original morphology upon the same treatment. At varying mass ratios of InN-NWs and GO, the different morphologies and distributions of In_2O_3 could be obtained on graphene sheets. The uniform distribution, which is usually considered favorable for enhanced sensing performance, was observed in In_2O_3 cubes/reduced graphene oxide (rGO) composites. The room-temperature NO_2 sensing properties of the In_2O_3 cubes/rGO composites-based sensor were systematically investigated. The results revealed that the sensor exhibited a significant response to NO_2 gas with a concentration lower to 1 ppm, and an excellent selectivity, even though the concentrations of interferential gases were 1000 times that of NO_2. The enhanced NO_2 sensing performances were attributed to the synergistic effect of uniformly distributed In_2O_3 cubes and graphene sheets in the unique hybrid architectures without the interfering of extra additives.

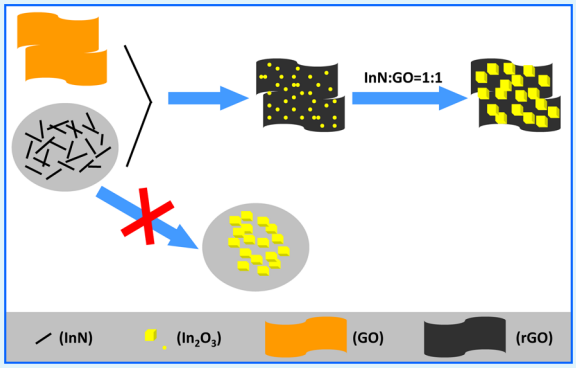

KEYWORDS: *In_2O_3 cubes, precursor, graphene oxide, sensing performance, synergistic effect*

1. INTRODUCTION

Graphene-based materials have been considered as distinctive building blocks for fabrication of gas sensors because of their unique two-dimensional (2D) structures and physical properties, such as fast electron transport kinetics, high specific surface area, etc.[1−4] In despite of such outstanding behaviors, pristine graphene materials themselves usually exhibit unsatisfied sensing properties, such as relatively low sensitivity, and poor reversibility.[5−7] Many efforts have been devoted to improve the sensing performance of graphene materials, including thermal treatment,[8] chemical modification,[9−12] microwave,[13] and UV irradiation treatment.[14] Among all these methods, the chemical modification approach attracted the most intensive attention because of the fact that it can be performed on a large scale at a relatively low cost.[15,16] Furthermore, during the process of chemical modification, functional micro/nanomaterials could be incorporated into graphene networks to form hybrid composites, which have been proven to be an effective way to improve the sensing performances because of the diverse functionalities and synergistic effect in the composites.[17−20] Physical mixing of pristine graphene materials and well-functionalized micro/nanomaterials is apparently the most convenient way for the formation of hybrid composites.[21] Unfortunately, this simple combination usually induces a severe aggregation and nonuniform distribution of functionalized micro/nanomaterials in graphene networks, subsequently leading a degradation of gas-sensing performances. The hydrothermal treatment of graphene oxide and metal salt solution has been considered as a facile and effective method to obtain uniformly distributed micro/nanomaterials with specific morphologies in the graphene networks.[19,20] Generally, the good sensing performances are accompanied by uniform distribution and ideal morphologies of the functional micro/nanomaterials.[22,23] Extra additives (surfactants or polymers), such as CTAB, SDS, PEG, etc., are usually applied to tune their morphologies and distribution during the hydrothermal

Received: September 2, 2014
Accepted: November 17, 2014
Published: November 17, 2014

process.[24−26] However, it is a tedious task to remove the additives after the synthesis, and the residual additives in the composites not only hinder the gas penetrating but influence the electronic conductivity of the hybrid structures, thus inducing a poor sensing performance.[27,28] Therefore, it is highly desirable to develop an additive-free synthesis of uniformly distributed functional micro/nanomaterials on graphene sheets.

Indium oxide (In_2O_3), as a typical wide-bandgap *n*-type semiconductor, has exhibited promising applications in gas sensors.[29] Up to now, various morphologies and functionalities of In_2O_3 micro/nanomaterials have been developed.[30] However, to the best of our knowledge, there are no available reports about the combination of In_2O_3 with graphene as sensing materials.

In this work, we report an additive-free synthesis of In_2O_3 cubes uniformly embedded into graphene sheets with InN nanowires (InN-NWs) and GO as precursors by a facile one-step microwave-assisted hydrothermal method. Without the help of graphene sheets, the bare InN-NWs precursor cannot transform to In_2O_3, and basically maintained their chemical composition and original morphology upon the same treatment. When InN-NWs and GO at varying mass ratios were applied as precursors, the different morphologies and distribution of In_2O_3 were achieved on graphene sheets. The uniform distribution, which is usually considered favorable for enhanced sensing performance, was observed in In_2O_3 cubes/rGO composites. The as-fabricated sensor based on In_2O_3 cubes/rGO composites exhibited an excellent selectivity and a significant response to NO_2 at a concentration lower to 1 ppm at room temperature.

2. EXPERIMENTAL SECTION

Material Synthesis. Graphene oxide (GO) was synthesized from purified graphite powder according to the modified Hummers method.[31] The purified GO were then dispersed in distilled water to make a 2 mg/mL solution. Exfoliation of GO was achieved by ultrasonication using an ultrasonic bath (Kudos, SK5200H, 200 W, China). InN-NWs were prepared by chemical vapor deposition (CVD) method (see the Supporting Information, Figure S1).[32] The In_2O_3/rGO composites were prepared by microwave-assisted hydrothermal method. In a typical preparation process, 1 mL of GO aqueous suspensions (2 mg/mL) was added into 9 mL of distilled water, and was sonicated for 30 min. Subsequently, the varying mass of InN-NWs was added into the above GO solution, and a well-dispersed solution was obtained by ultrasonication for 1 min. After that, the uniform dispersion was sealed in a 100 mL Teflon container and transferred into a microwave digestion system (SINEO, MDS-6G, China). The reaction was then preformed at 150 °C for 30 min under microwave irradiation (2450 ± 50 MHz). After cooling to room temperature naturally, the resulting products were cleaned by centrifugation/washing cycles with distilled water for three times, and then air-dried at 100 °C for 24 h. In our experiment, the mass ratios of InN-NWs and GO were controlled as 0.1:1, 0.5:1, 1:1, 3:1, and 5:1, respectively. For comparison, individual InN-NWs and GO were separately conducted by the same procedure without any other additives.

Characterizations. X-ray powder diffraction (XRD) was performed on a Rigaku D/Max 2500 diffractometer with Cu K_α1 radiation (λ = 0.15406 nm). The samples were scanned at a rate of 5°/min over the 2θ range of 5−65°. The morphologies of the as-obtained samples were characterized by field-emission SEM (Nova NanoSEM 450, FEI) with an accelerating voltage of 3 kV. Raman spectra were recorded on a Raman confocal microspectrometer (HR-800, Jobin-Yvon, Horiba, France) excited by a He−Ne laser (632.8 nm, 13.6 mW). Fourier-transform infrared (FT-IR) spectra of KBr powder pressed pellets were recorded on a Spectrum 100 FT-IR (PerkinElmer Instrument Co.) with a scan range of 4000−400 cm^{-1}. X-ray photoelectron spectroscopy (XPS) analysis was carried out on an ESCALAB250 spectrometer (Thermo VG Co, USA) with Al K_α (1486.6 eV) as X-ray radiation.

Fabrication and Gas-Sensing Measurements. For fabricating the sensing devices, the sensing materials were dispersed in absolute ethanol by ultrasonication, and then the mixed solution was dropped onto a ceramic plate (1.0 × 1.5 mm) which was previously mounted a pair of gold electrodes on the frontal sides by screen printing technique (see the Supporting Information, Figure S2), followed by drying at room temperature. The gas-sensing measurements were carried out in a 100 mL homemade testing chamber. A gas mixing line equipped with mass flow controllers (MFCs) was designed to prepare the NO_2 at specific concentrations and relative humidity (RH) in the testing chamber (see the Supporting Information, Figure S3).[33,34] The resistance changes of sensor in air or tested gas were monitored by a high-resistance meter (Victor, 86E, China), and the response signal (S) of gas sensor was defined as the R_a/R_g (for oxidizing gas), or R_g/R_a (for reducing gas) ratio (R_a, resistance in air; R_g, resistance in tested gas). Before sensing measurements, the chamber was purged with air until a constant resistance was obtained. The sensor was then exposed to NO_2 and air flow alternately.

3. RESULTS AND DISCUSSION

InN-NWs and GO at different mass ratios, as well as individual InN-NWs and GO, were conducted by the microwave-assisted hydrothermal reaction. The chemical composition of the products obtained before and after microwave-assisted hydrothermal reaction was analyzed by XRD technique.

Figure 1a shows the typical XRD patterns of GO. A strong peak at 2θ of 10.64° corresponding to the (001) plane is clearly

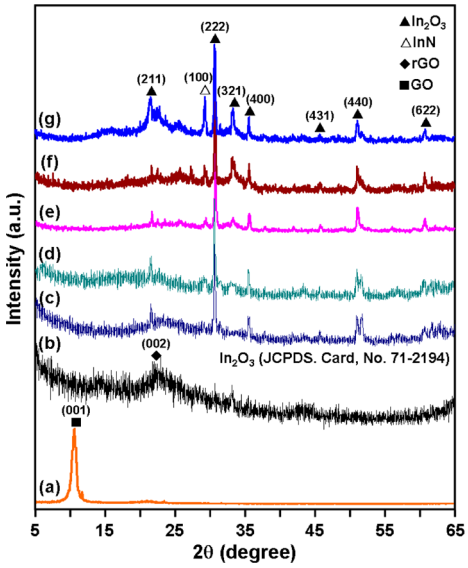

Figure 1. Typical XRD patterns of (a) GO, (b) rGO, and the as-obtained In_2O_3/rGO composites with various mass ratios of InN-NWs and GO as precursors: (c) 0.1:1, (d) 0.5:1, (e) 1:1, (f) 3:1, and (g)5:1 by microwave-assisted hydrothermal reaction at 150 °C for 30 min.

observed, indicating the successful preparation of GO by oxidation of the graphite powder.[19] For the XRD pattern of rGO prepared by reduction of bare GO, as shown in Figure 1b, the peak at 10.64° disappears and a broad peak appears at approximately 22.2°, confirming the conversion of GO to rGO after the microwave-assisted hydrothermal reaction.[35] Figure 1c-g illustrates the XRD patterns of the five composites prepared from InN-NWs and GO at varying mass ratios. None of obvious typical peaks belonging to rGO are observed in

these XRD patterns. This implies that the graphene sheets are highly disordered stacking with a low degree of graphitization and the existence of In_2O_3 in the composites prevents the graphene sheets from restacking.[27] Furthermore, except for the diffraction peak marked with Δ, which is originated from (100) plane of InN (JCPDS Card, No. 50−1239), all the other detectable peaks are indexed as cubic phase In_2O_3 (JCPDS Card, No. 71−2194). This indicates that InN could be transformed to In_2O_3 in the presence of the graphene sheets by the microwave-assisted hydrothermal reaction. Although the amount of residual InN in the In_2O_3/rGO composites is very tiny, it is still noteworthy that along with the increase of the mass ratio of InN-NWs and GO, the relative diffraction peak intensity of the (100) plane from InN is gradually enhanced. In contrast, without the addition of GO, InN-NWs were hydrolyzed very slowly and basically maintained their chemical composition and original morphologies upon the same microwave treatment (see the Supporting Information, Figure S4). As a proof of concept, the existence of graphene sheets plays a vital role in the conversion from InN to In_2O_3 during the microwave-assisted hydrothermal process.

The morphologies of the as-obtained In_2O_3 cubes/rGO composites with InN-NWs and GO as precursors (mass ratio was 1:1) were further investigated by SEM, as shown in Figure 2. Observed from the SEM image in Figure 2a, the graphene sheets exhibit a clean and transparent film, and the In_2O_3 cubes are uniformly embedded into graphene networks, indicating an effective strategy to incorporate In_2O_3 cubes into graphene sheets by one-step microwave-assisted hydrothermal method. The enlarged-magnification SEM image is shown in Figure 2b, and reveals clearly defined and well-faceted In_2O_3 cubes with size of 50−250 nm. Furthermore, the crumpled graphene sheets with many folds and wrinkles (as indicated by green arrows in Figure 2b) provide extremely high surface area, thus facilitating the effective access of gases to the In_2O_3 surfaces.[27]

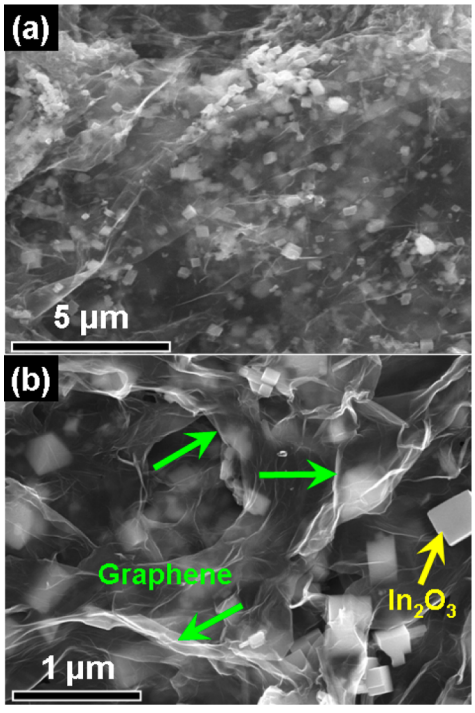

Figure 2. (a, b) SEM images of the In_2O_3 cubes/rGO composites with InN-NWs and GO as precursors (mass ratio was 1:1) at different magnification.

To investigate the effect of InN-NWs precursor amount in the GO solution on the morphologies and distribution of In_2O_3 on graphene sheets, we carried out the controlled experiments with varying mass ratios of InN-NWs and GO (0.1:1, 0.5:1, 3:1 and 5:1) under the same experimental condition. SEM images of the as-prepared In_2O_3/rGO composites are shown in Figure 3. When the mass ratio of InN-NWs and GO was controlled at 0.1:1, many amorphous In_2O_3 particles were observed and tended to aggregate to clusters, as shown in Figure 3a. When the mass ratio of InN-NWs and GO enhanced to 0.5:1, the bulk In_2O_3 were found (Figure 3b). As this ratio kept increasing (3:1), a mixture of particles and nanowires were obtained in the composites (Figure 3c). Meanwhile, it can be obviously seen that some isolated particles deposited on the surface of the nanowires, and the nanowires showed a coarse surface and a noticeable fluctuation in diameter along their longitudinal axes. When the mass ratio of InN-NWs and GO increased to 5:1, more In_2O_3 nanowires and less particles were observed in the composites (Figure 3d).

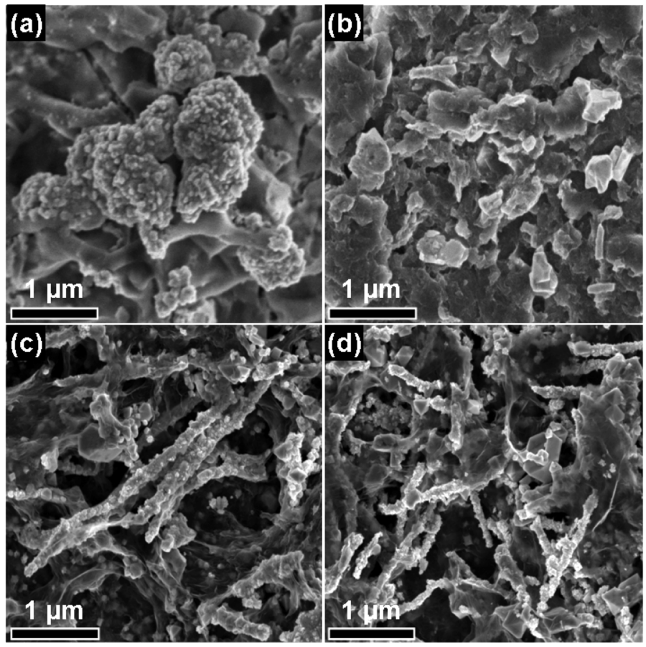

Figure 3. SEM images of the In_2O_3/rGO composites with different mass ratio of InN-NWs and GO as precursors: (a) 0.1:1; (b) 0.5:1; (c) 3:1; (d) 5:1.

A tentative explanation on the formation and growth of In_2O_3 with various morphologies in the composites are schematically illustrated in Figure 4. As mentioned previously, the additives (surfactant or polymers) are usually introduced to the synthesis process, and these additives not only help the dispersion of different matrices but tune the morphologies of products.[25,26] Without additives, the precursors and newly generated nano/micromaterials may separate from the solution phase and form precipitation. However, in our case, the GO sheets themselves contain both the hydrophobic basal plane and hydrophilic edges, which can also be considered as a surfactant.[36] Furthermore, their basal planes are decorated mostly with epoxy and hydroxyl groups, while carbonyl and carboxyl groups are located at the edges, representing as anchor

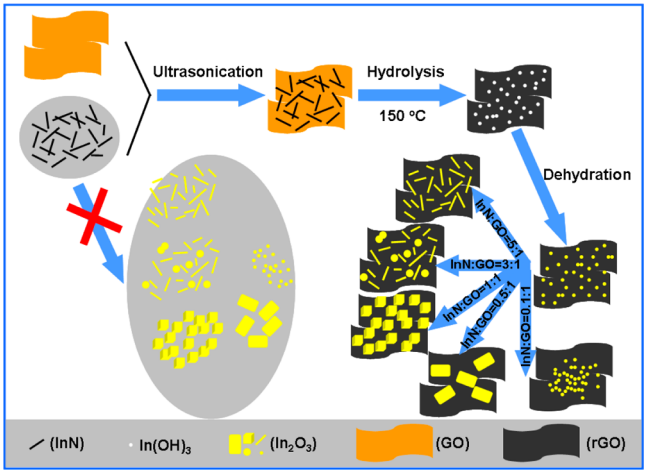

Figure 4. Schematic illustration of the formation process of the In_2O_3/rGO composites.

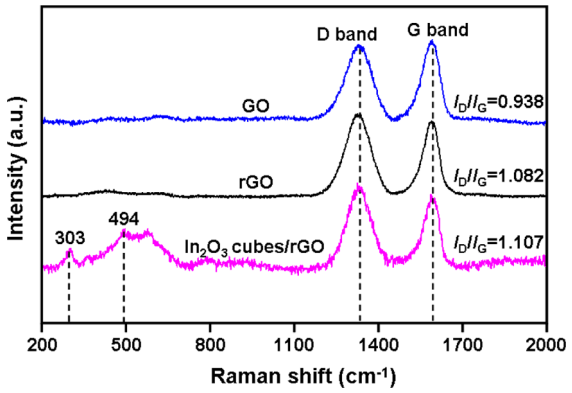

Figure 5. Raman spectra of GO, rGO, and In_2O_3 cubes/rGO composites.

sites.[37] Therefore, in the presence of the GO, the InN-NWs precursor could be well-dispersed in the solution homogeneously (see the Supporting Information, Figure S5).[38] Meanwhile, in the presence of GO, the InN-NWs tend to be hydrolyzed and decomposed into In_2O_3 crystal nucleus in the process of microwave-assisted hydrothermal treatment. Simultaneously, the insulating GO is reduced into conductive rGO, which has been reported as the nucleation sites for further crystal growth.[19] These generated In_2O_3 crystal nuclei spontaneously aggregate into large assemblages to minimize their surface energy, thus leading different morphologies.[39]

The concentration of In_2O_3 crystal nuclei in the solution shows a significant influence on the final In_2O_3 morphology in graphene networks.[19] With less concentration of In_2O_3 crystal nuclei, as examples in Figure 3a, b, they tend to aggregate and form bulk In_2O_3. However, with suitable concentration of In_2O_3 crystal nuclei, as the example in our case of Figure 2a, b, they tend to be nucleated and evolve into cube morphology through Ostwald ripening process in the composites.[39,40] In contrast, as the concentration of In_2O_3 crystal nuclei increases (e.g., Figure 3c), the fast growth facilitates the appearance of nonuniform nanowires, with irregular nanoparticles loading on the surfaces of the nanowires.[18] Furthermore, the corrugated rGO sheets form in the hydrothermal process, resulting that partial In_2O_3 nanoparticles are wrapped with the rGO sheets. As the concentration of In_2O_3 crystal nuclei keeps increasing (e.g., Figure 3d), more and more nanoparticles transform to wire-like shapes by self-assemble, leading the appearance of more In_2O_3 nanowires in the composites.

It was noteworthy that the as-generated In_2O_3 with diverse shapes and sizes showed different effects on their distribution in the graphene networks.[38] The amorphous particles, bulk In_2O_3, and nanowires all exhibited a relatively nonuniform distribution on the graphene sheets, while the In_2O_3 cubes were uniformly embedded into graphene networks. As mentioned previously, the ideal sensing performance is usually accompanied by uniform distribution of sensing materials.[22,23] Therefore, we focused on the In_2O_3 cubes/rGO composites for further characterizations and used as the gas-sensing material.

The reduction of GO and the formation of In_2O_3 in In_2O_3 cubes/rGO composites are further confirmed by using Raman spectra. The Raman spectra of GO, rGO, and the In_2O_3 cubes/rGO composites are illustrated in Figure 5. It is obviously seen that all three samples exhibit two major peaks, containing the D band at 1340 cm^{-1} and the G band at 1595 cm^{-1}.[19] The G-band is ascribed to the first-order scattering of the E2g mode.[19] The D-band is associated with the structural defects, which are related to the partially disordered structures of graphitic domains or created by the attachments of functional groups on the carbon basal plane.[41] Furthermore, the intensity ratios of the D to the G band (I_D/I_G) for rGO and In_2O_3 cubes/rGO composites are 1.082 and 1.107, respectively, which is higher than that of GO (0.938). These results demonstrate the formation of new graphitic domains for both rGO and In_2O_3 cubes/rGO composites after the microwave-assisted hydrothermal process.[42] Additionally, for Raman spectra of the In_2O_3 cubes/rGO composites, there are two peaks at 303 and 494 cm^{-1}, which could be assigned to the characteristic modes of cubic In_2O_3.[43] This also indicates the formation of In_2O_3 in the composites after the microwave-assisted hydrothermal treatment. Similar results were observed in FT-IR spectrum (see the Supporting Information, Figure S6).

To further characterize the as-obtained products, we conducted the surface composition and element analysis by X-ray photoelectron spectroscopy (XPS) technique. Figure 6a exhibits the XPS survey spectra of GO, rGO and In_2O_3 cubes/rGO composites, revealing two peaks at 284 and 531 eV, which can be attributed to C 1s and O 1s, respectively.[20] Furthermore, In_2O_3 cubes/rGO composites exhibit several bands associated with In element (In 3p, 3d, 4d), indicating the presence of In element in the hybrid architecture.[29] In the case of rGO, the C/O atomic ratio is 4.061, which is much higher than that of GO (2.145). This increase of the C/O atomic ratio in rGO demonstrates that microwave-assisted hydrothermal method is capable of eliminating most of the oxygen-containing functional groups of GO.[42] However, the C/O atomic ratio in In_2O_3 cubes/rGO composites is 2.619, which is lower than that of individual rGO but higher than that of GO (see the Supporting Information, Table S1). This could be ascribed to the reduction of GO and the incorporation of In_2O_3 into graphene networks. Except the O binding with In, the C/O atomic ratio of rGO in In_2O_3 cubes/rGO is 4.322, indicating a similar reduction degree of GO in both the bare rGO (4.061) and In_2O_3 cubes/rGO composites upon the same treatment (see the Supporting Information, Table S1). In 3d XPS spectra of In_2O_3 cubes/rGO composites have two strong peaks with binding energy at 451.4 eV ($In\ 3d_{3/2}$) and 443.8 eV ($In\ 3d_{5/2}$), as shown in Figure 6b, demonstrating the formation of In_2O_3 in the composites.[29] Furthermore, C 1s spectra of GO and In_2O_3 cubes/rGO

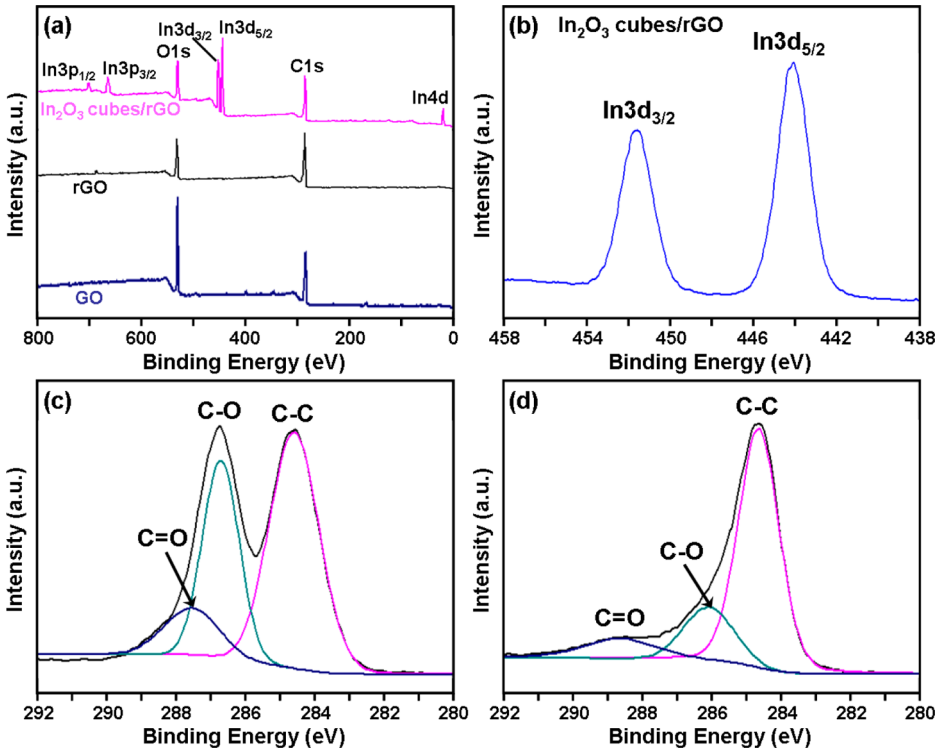

Figure 6. (a) XPS survey spectra of GO, rGO, and In_2O_3 cubes/rGO composites; (b) In 3d spectrum of In_2O_3 cubes/rGO composites; (c) C 1s spectrum of GO, and (d) In_2O_3 cubes/rGO composites.

composites are shown in Figure 6c, d, respectively. Three peaks at 284.6, 286.7, and 288.5 eV are clearly observed, and are attributed to the C−C, C−O and C═O bands separately in the samples.[41] In contrast, a noticeable decrease in the peak intensity of C−O and C═O was achieved after microwave-assisted hydrothermal reaction, suggesting that most oxygen-containing functional groups are successfully removed in the microwave-assisted hydrothermal treatment.[20] As a result, these observations indicate the successful reduction of GO and the formation of In_2O_3 by microwave-assisted hydrothermal treatment of InN-NWs precursor in GO solution.

As mentioned above, both the uniform distribution of In_2O_3 cubes in graphene networks, and the crumpled graphene sheets with numerous wrinkles and folds in the hybrid architectures are advantageous for gas-sensing applications.[27] Therefore, in our experiment, we fabricated a gas sensor using the In_2O_3 cubes/rGO composites, and evaluated its sensing performance. NO_2 gas was selected as the target gas since it is the most dangerous air pollutant to plants and respiratory system of human beings and animals. In addition, it threatens environmental security as a source of photochemical smog and acid rain.[26,33] Thus, the detection of NO_2 has attracted extensive interest in health and environmental monitoring.

Figure 7a shows the dynamic resistance changes of the as-fabricated In_2O_3 cubes/rGO-based sensor to various concentrations of NO_2 under 50% RH at room temperature. The sensor resistances decreased with the exposure of NO_2, indicating the *p*-type response of the senor.[35] The sensing time of each NO_2 concentration was fixed at 3 min for further measurements and comparison. Furthermore, as the NO_2 concentration goes up, the resistances of the sensor keeps decreasing obviously. A linear fitting curve of the sensor response versus the NO_2 concentration in the range of 1 to 15 ppm is obtained, as shown in Figure 7b, and the correlation

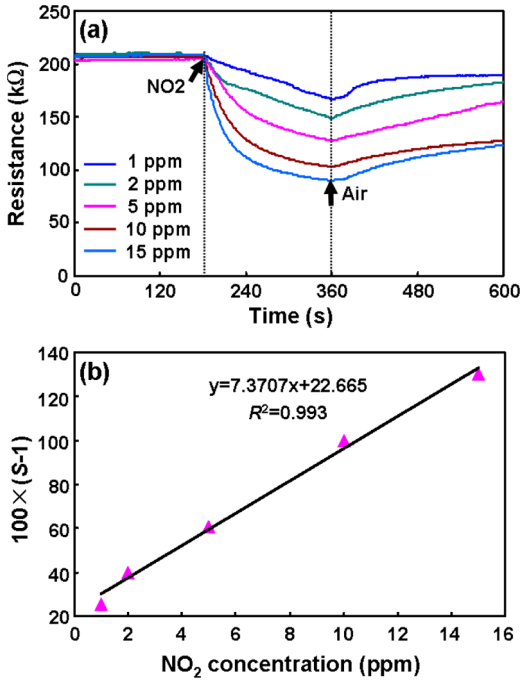

Figure 7. (a) Dynamic resistance changes of the sensor based on In_2O_3 cubes/rGO composites to various concentrations of NO_2 under 50% RH at room temperature; (b) linear fitting curve of the sensor response versus NO_2 concentration.

coefficient R^2 of the fitting curve is 0.993, indicating a good linearity.

For comparison, pure In_2O_3-based and rGO-based sensors were fabricated separately using the same amount of sensing materials and exactly same fabricated procedure. The sensing

properties of these sensors to NO_2 at 50% RH and room temperature were compared. It is clearly seen that the In_2O_3 cubes/rGO-based sensor displays the highest response among these three sensors (see the Supporting Information, Figure S7). Such observations indicate that the combination of In_2O_3 cubes and rGO significantly enhances the NO_2-sensing performances of rGO-based sensor.

To further evaluate the response and recovery characteristic, the sensing performances of the as-fabricated In_2O_3 cubes/rGO-based sensor to 5 ppm of NO_2 under 50% RH at room temperature, 50, 80, 110 °C are also investigated, respectively. The elevated working temperature leads relatively shorter recovery time, but lower sensor responses (see the Supporting Information, Figure S8). As we mentioned, for the safety concern in some specific atmosphere, such as inflammable and explosive environments, we evaluate the sensing properties of as-prepared sensor at room temperature.

The repeatability of our sensing devices was also investigated. The In_2O_3 cubes/rGO-based sensor was exposed to 5 ppm of NO_2 for 3 min under 50% RH at room temperature for five response cycles. Although the recovery time in air is relatively long (Figure 7), once the sensor gets refreshed, it still exhibits good repeatability. As shown in Figure 8, all five response cycles

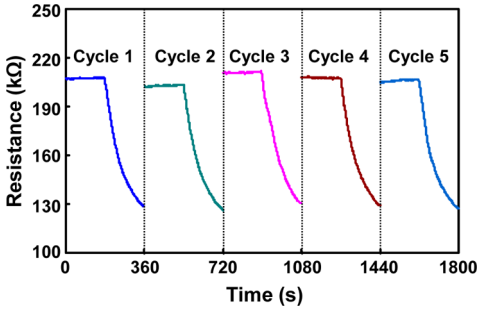

Figure 8. Resistance changes of the In_2O_3 composites-based sensor during five cycles of exposure to 5 ppm of NO_2 for 3 min under 50% RH at room temperature.

present very similar trends after exposure to NO_2. The long-term stability of the sensor was evaluated by exposure the sensor to 5 ppm of NO_2 under 50% RH at room temperature for a period of 2 weeks (see the Supporting Information, Figure S9), and the sensor exhibits good stability and only less than 3% variation is observed.

Selectivity is also an important parameter for gas sensor in practical applications. Figure 9 reveals the cross-response of the

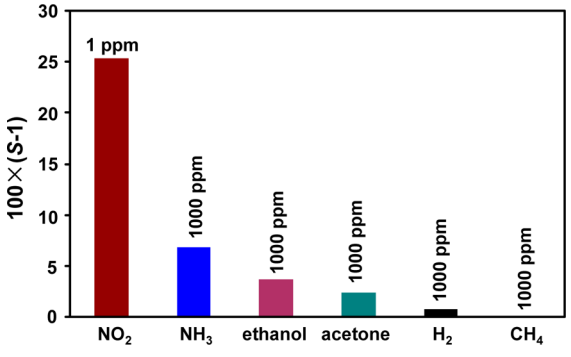

Figure 9. Response of the In_2O_3 cubes/rGO composites-based sensor to various tested gas under 50% RH at room-temperature.

In_2O_3 cubes/rGO composites-based sensor to several possible interferential gases, including ammonia, ethanol, acetone, hydrogen, and methane. It is clearly observed that the sensor exhibits the largest response to NO_2 among these gases, even though the concentration of the other tested gases are 1000 times that of NO_2. Such results indicate that the sensor exhibits an excellent selectivity toward NO_2 under 50% RH at room temperature. This enhanced selectivity could be explained by the selective adsorption of NO_2 on rGO. NO_2 is an electron-withdrawing molecule, tending to adsorb on electron-rich sites such as the lone-pair electrons of O atoms in oxygen-containing functional groups of rGO.[5] The chemically modified rGO (In_2O_3/rGO) contains defect sites and functional groups, which could act as highly active centers for NO_2.[46] After NO_2 adsorption, the electron-withdrawing abilities of the oxygen-containing functional groups and defects are enhanced. And consequently, the resistance of the *p*-type In_2O_3/rGO sensing layer decreased significantly.

A comparison of the sensor responses to NO_2 in the present work and literature reports is summarized in Table 1.[7,44−48] It is noteworthy that the as-fabricated sensor in our work exhibits better sensing performances compared with those reported previously in the literature. Although there exist some In_2O_3-based NO_2 sensors with larger sensitivity (R_g/R_a),[26,49,50] the high operating temperature limit their practical applications. Thus, our sensor is still a promising candidate for detecting NO_2 gas at room temperature.

The sensing mechanism of the sensor based on the In_2O_3 cubes/rGO composites is further discussed. As we all know, vacancies and defects are the major charge carriers for typical *p*-type rGO semiconductor,[44] whereas In_2O_3 is an *n*-type semiconductor with free electrons as major charge carriers.[22] The effective electronic interaction between In_2O_3 cubes and rGO facilitates the gas molecule detection via the resistance change of the hybrid architectures.[18] In ambient air, oxygen molecules are directly adsorbed onto the surface and capture free electrons from the conductance band of the composites to generate chemisorbed oxygen species, leading a high-resistance depletion layer.[22] When the sensor is exposed to NO_2, the high electrophilic NO_2 molecules not only capture the electrons from the conductance band, but also react with the absorbed oxygen species.[26] Such adsorption and reaction further capture the electrons from the *p*-type In_2O_3 cubes/rGO composites, resulting in an increase of the charge carrier concentration, which eventually decrease the sensor resistance.[44] When the sensor is exposed in air again, the absorbed NO_2 species are desorbed, leading a recovery of the initial condition.

The enhanced sensing performance of the In_2O_3 cubes/rGO composites is tentatively explained from the following aspects. First, an additive-free synthesis is developed to avoid the introduction of extra additives, which not only hinder the gas penetrating but influence the electronic conductivity of the composites.[28] Second, the uniform distribution of In_2O_3 cubes in the graphene networks guarantees the good gas penetration and transport in the composites.[22] Third, the existence of graphene sheets in the hybrid architectures overcomes the poor electrical conductivity of In_2O_3 at room temperature. Finally, the graphene sheets with many overlapped and crumpled regions provide high surface areas, thus facilitating the effective access of gases to the In_2O_3 surfaces.[27] Therefore, the enhanced sensing performance for NO_2 at room temperature could be achieved by using as-obtained In_2O_3 cubes/rGO composites.

Table 1. Detection of NO_2 Using Graphene-Based Sensors[a]

sensing materials	additives	NO_2 (ppm)	operating temperature	response
Al-decorated graphene[7]	[b]	1.2	150 °C	$(R_a - R_g)/R_a$ = 2.89%
Ag-S-RGO[44]	Na_2CO_3, $NaBH_4$, sulfanilic acid, $NaNO_2$, $AgNO_3$, HCl, hydrazine	5	RT	$(R_a - R_g)/R_a$ = 16.7%
ethanol-based CVD graphene nanomesh[45]	polystyrene, SDS	10	RT	$(R_a - R_g)/R_a$ = 11%
nontreated graphene[46]	SDS	5	RT	$(G - G_0)/G_0$ = 11.17% (calcd: $(R_a - R_g)/R_a$ = 10.05%)
flexible RGO[47]	CH, EDC, NHS, $NaBH_4$	5	RT	$(R_a - R_g)/R_a$ = 12%
ozone-treated graphene[48]	[b]	5	RT	$(R_a - R_g)/R_a$ = 3.7%
In_2O_3cubes/rGO (our work)	[c]	5	RT	$(R_a/R_g - 1$ = 60.80% (calcd: $(R_a - R_g)/R_a$ = 37.81%)

[a]SDS, sodium dodecyl sulfate; CH, cysteamine hydrochloride; EDC, *N*-(3-(dimethylamino)propyl)-N′-ethylcarbodiimide hydrochloride; NHS, *N*-hydroxysuccinimide; RT, room temperature. [b]Sensing materials prepared by CVD growth method. [c]Nonadditive, except InN and GO.

4. CONCLUSION

In summary, we have developed an additive-free synthesis of In_2O_3 cubes uniformly embedded into graphene networks by a facile one-step microwave-assisted hydrothermal method. The InN-NWs and GO were utilized as precursors. In absence of GO, the InN-NWs precursor nearly maintained their chemical composition and original morphology under the same condition. After varying the mass ratios of InN-NW and GO, different morphologies and distribution of In_2O_3 were obtained in the In_2O_3/rGO composites. The uniform distribution, which is usually considered favorable for enhanced gas sensing performance, was observed in In_2O_3 cubes/rGO composites. The as-fabricated sensor based on In_2O_3 cubes/rGO composites exhibited a significant response to NO_2 gas with a concentration lower to 1 ppm at room temperature. An excellent selectivity was also achieved, even though the concentrations of interferential gases were 1000 times that of NO_2. The enhanced NO_2 sensing performances were attributed to the synergistic effect of uniformly distributed In_2O_3 cubes and graphene sheets in the unique hybrid architectures without the interfering of extra additives.

■ ASSOCIATED CONTENT

Supporting Information

Photograph of the as-prepared InN-NWs in a quartz boat, the sensor, and homemade testing system. SEM images and EDS analysis of InN-NWs before and after the microwave-assisted hydrothermal treatment. Optical images of GO solution (0.1 mg/mL), InN power dispersed in 0.1 mg/mL GO solution, and the as-obtained In_2O_3/rGO composites. FT-IR and XPS analysis of GO, rGO, and the In_2O_3 cubes/rGO composites. This material is available free of charge via the Internet at http://pubs.acs.org.

■ AUTHOR INFORMATION

Corresponding Author

*E-mail: fengl@dicp.ac.cn. Tel. & Fax: +86 411 84379411.

Notes

The authors declare no competing financial interest.

■ ACKNOWLEDGMENTS

The work was supported through the National Natural Science Foundation of China (Grant 21177125, 21321064) and the 100 talents program, which is funded by Chinese Academy of Sciences.

■ REFERENCES

(1) Schedin, F.; Geim, A. K.; Morozov, S. V.; Hill, E. W.; Blake, P.; Katsnelson, M. I.; Novoselov, K. S. Detection of Individual Gas Molecules Adsorbed on Graphene. *Nat. Mater.* **2007**, *6*, 652−655.

(2) Li, W. W.; Geng, X. M.; Guo, Y. F.; Rong, J. Z.; Gong, Y. P.; Wu, L. Q.; Zhang, X. M.; Li, P.; Xu, J. B.; Cheng, G. S.; Sun, M. T.; Liu, L. W. Reduced Graphene Oxide Electrically Contacted Graphene Sensor for Highly Sensitive Nitric Oxide Detection. *ACS Nano* **2011**, *5*, 6955−6961.

(3) Dua, V.; Surwade, S. P.; Ammu, S.; Agnihotra, S. R.; Jain, S.; Roberts, K. E.; Park, S.; Ruoff, R. S.; Manohar, S. K. All-Organic Vapor Sensor Using Inkjet-Printed Reduced Graphene Oxide. *Angew. Chem., Int. Ed.* **2010**, *49*, 2154−2157.

(4) Robinson, J. T.; Perkins, F. K.; Snow, E. S.; Wei, Z. Q.; Sheehan, P. E. Reduced Graphene Oxide Molecular Sensors. *Nano Lett.* **2008**, *8*, 3137−3140.

(5) Yuan, W. J.; Liu, A. R.; Huang, L.; Li, C.; Shi, G. Q. High-performance NO_2 Sensors Based on Chemically Modified Graphene. *Adv. Mater.* **2013**, *25*, 766−771.

(6) Lu, G. H.; Park, S.; Yu, K. H.; Ruoff, R. S.; Ocola, L. E.; Rosenmann, D.; Chen, J. H. Toward Practical Gas Sensing with Highly Reduced Graphene Oxide: A New Signal Processing Method To Circumvent Run-to-Run and Device-to-Device Variations. *ACS Nano* **2011**, *5*, 1154−1164.

(7) Cho, B.; Yoon, J.; Hahm, M. G.; Kim, D.-H.; Kim, A. R.; Kahng, Y. H.; Park, S.-W.; Lee, Y.-J.; Park, S.-G.; Kwon, J.-D.; Kim, C. S.; Song, M.; Jeong, Y.; Nam, K.-S.; Ko, H. C. Graphene-based Gas Sensor: Metal Decoration Effect and Application to a Flexible Device. *J. Mater. Chem. C* **2014**, *2*, 5280−5285.

(8) Wang, Z. L.; Xu, D.; Huang, Y.; Wu, Z.; Wang, L. M.; Zhang, X. B. Facile, Mild and Fast Thermal-Decomposition Reduction of Graphene Oxide in Air and its Application in High-Performance Lithium Batteries. *Chem. Commun.* **2012**, *48*, 976−978.

(9) Dey, R. S.; Hajra, S.; Sahu, R. K.; Raj, C. R.; Panigrahi, M. K. A Rapid Room Temperature Chemical Route for the Synthesis of Graphene: Metal-Mediated Reduction of Graphene Oxide. *Chem. Commun.* **2012**, *48*, 1787−1789.

(10) Kumar, N. A.; Gambarelli, S.; Duclairoir, F.; Bidan, G.; Dubois, L. Synthesis of High Quality Reduced Graphene Oxide Nanosheets Free of Paramagnetic Metallic Impurities. *J. Mater. Chem. A* **2013**, *1*, 2789−2794.

(11) Zhu, C. Z.; Guo, S. J.; Fang, Y. X.; Dong, S. J. Reducing Sugar: New Functional Molecules for the Green Synthesis of Graphene Nanosheets. *ACS Nano* **2010**, *4*, 2429−2437.

(12) Ghosh, R.; Midya, A.; Santra, S.; Ray, S. K.; Guha, P. K. Chemically Reduced Graphene Oxide for Ammonia Detection at Room Temperature. *ACS Appl. Mater. Interfaces* **2013**, *5*, 7599−7603.

(13) Chen, W. F.; Yan, L. F.; Bangal, P. R. Preparation of Graphene by the Rapid and Mild Thermal Reduction of Graphene Oxide Induced by Microwaves. *Carbon* **2010**, *48*, 1146−1152.

(14) Ding, Y. H.; Zhang, P.; Zhuo, Q.; Ren, H. M.; Yang, Z. M.; Jiang, Y. A Green Approach to the Synthesis of Reduced Graphene Oxide Nanosheets under UV Irradiation. *Nanotechnology* **2011**, *22*, 215601.
(15) Chua, C. K.; Pumera, M. Chemical Reduction of Graphene Oxide: A Synthetic Chemistry Viewpoint. *Chem. Soc. Rev.* **2014**, *43*, 291−312.
(16) Pei, S. F.; Cheng, H. M. The Reduction of Graphene Oxide. *Carbon* **2012**, *50*, 3210−3228.
(17) Deng, S.; Tjoa, V.; Fan, H. M.; Tan, H. R.; Sayle, D. C.; Olivo, M.; Mhaisalkar, S.; Wei, J.; Sow, C. H. Reduced Graphene Oxide Conjugated Cu_2O Nanowire Mesocrystals for High-Performance NO_2 Gas Sensor. *J. Am. Chem. Soc.* **2012**, *134*, 4905−4917.
(18) An, X. Q.; Yu, J. C.; Wang, Y.; Hu, Y. M.; Yu, X. L.; Zhang, G. J. WO_3 Nanorods/Graphene Nanocomposites for High-Efficiency Visible-Light-Driven Photocatalysis and NO_2 Gas Sensing. *J. Mater. Chem.* **2012**, *22*, 8525−8531.
(19) Guan, Q.; Cheng, J. L.; Wang, B.; Ni, W.; Gu, G. F.; Li, X. D.; Huang, L.; Yang, G. C.; Nie, F. D. Needle-like Co_3O_4 Anchored on the Graphene with Enhanced Electrochemical Performance for Aqueous Supercapacitors. *ACS Appl. Mater. Interfaces* **2014**, *6*, 7626−7632.
(20) Wang, Z. Y.; Xiao, Y.; Cui, X. B.; Cheng, P. F.; Wang, B.; Gao, Y.; Li, X. W.; Yang, T. L.; Zhang, T.; Lu, G. Y. Humidity-Sensing Properties of Urchinlike CuO Nanostructures Modified by Reduced Graphene Oxide. *ACS Appl. Mater. Interfaces* **2014**, *6*, 3888−3895.
(21) Zhu, X.; Song, X. Y.; Ma, X. L.; Ning, G. Q. Enhanced Electrode Performance of Fe_2O_3 Nanoparticle-Decorated Nanomesh Graphene as Anodes for Lithium-Ion Batteries. *ACS Appl. Mater. Interfaces* **2014**, *6*, 7189−7197.
(22) Tricoli, A.; Righettoni, M.; Teleki, A. Semiconductor Gas Sensors: Dry Synthesis and Application. *Angew. Chem., Int. Ed.* **2010**, *49*, 7632−7659.
(23) Huang, J. R.; Xu, X. J.; Gu, C. P.; Yang, M.; Yang, M.; Liu, J. H. Large-Scale Synthesis of Hydrated Tungsten Oxide 3D Architectures by a Simple Chemical Solution Route and Their Gas-sensing Properties. *J. Mater. Chem.* **2011**, *21*, 13283−13289.
(24) Li, E.; Cheng, Z. X.; Xu, J. Q.; Pan, Q. Y.; Yu, W. J.; Chu, Y. L. Indium Oxide with Novel Morphology: Synthesis and Application in C_2H_5OH Gas Sensing. *Cryst. Growth Des.* **2009**, *9*, 2146−2151.
(25) Chen, Y. J.; Meng, F. N.; Yu, H. L.; Zhu, C. L.; Wang, T. S.; Gao, P.; Ouyang, Q. Y. Sonochemical Synthesis and ppb H_2S Sensing Performances of CuO Nanobelts. *Sens. Actuators, B* **2013**, *176*, 15−21.
(26) Xu, X. M.; Zhao, P. L.; Wang, D. W.; Sun, P.; You, L.; Sun, Y. F.; Liang, X. S.; Liu, F. M.; Chen, H.; Lu, G. Y. Preparation and Gas Sensing Properties of Hierarchical Flower-Like In_2O_3 Microspheres. *Sens. Actuators, B* **2013**, *176*, 405−412.
(27) Yang, S. H.; Song, X. F.; Zhang, P.; Sun, J.; Gao, L. Self-Assembled alpha-Fe_2O_3 Mesocrystals/Graphene Nanohybrid for Enhanced Electrochemical Capacitors. *Small* **2014**, *10*, 2270−2279.
(28) Liu, H. T.; Liu, Y. Q.; Zhu, D. B. Chemical Doping of Graphene. *J. Mater. Chem.* **2011**, *21*, 3335−3345.
(29) Du, N.; Zhang, H.; Chen, B. D.; Ma, X. Y.; Liu, Z. H.; Wu, J. B.; Yang, D. R. Porous Indium Oxide Nanotubes: Layer-by-Layer Assembly on Carbon-Nanotube Templates and Application for Room-Temperature NH_3 Gas Sensors. *Adv. Mater.* **2007**, *19*, 1641−1645.
(30) Fan, Y. J.; Li, Z. P. Fabrication and Gas Sensing Properties of One-Dimensional In_2O_3 Nanostructures. *J. Nanoeng. Nanomanuf.* **2012**, *2*, 123−132.
(31) Marcano, D. C.; Kosynkin, D. V.; Berlin, J. M.; Sinitskii, A.; Sun, Z. Z.; Slesarev, A.; Alemany, L. B.; Lu, W.; Tour, J. M. Improved Synthesis of Graphene Oxide. *ACS Nano* **2010**, *4*, 4806−4814.
(32) Schwenzer, B.; Loeffler, L.; Seshadri, R.; Keller, S.; Lange, F. F.; DenBaars, S. P.; Mishra, U. K. Preparation of Indium Nitride Micro- and Nanostructures by Ammonolysis of Indium Oxide. *J. Mater. Chem.* **2004**, *14*, 637−641.
(33) Lim, H. S.; Feng, L.; Kemling, J. W.; Musto, C. J.; Suslick, K. S. An Optoelectronic Nose for the Detection of Toxic Gases. *Nat. Chem.* **2009**, *1*, 562−567.
(34) Feng, L.; Musto, C. J.; Suslick, K. S. A Simple and Highly Sensitive Colorimetric Detection Method for Gaseous Formaldehyde. *J. Am. Chem. Soc.* **2010**, *132*, 4046−4047.
(35) Zhang, H.; Feng, J. C.; Fei, T.; Liu, S.; Zhang, T. SnO_2 Nanoparticles-Reduced Graphene Oxide Nanocomposites for NO_2 Sensing at Low Operating Temperature. *Sens. Actuators, B* **2014**, *190*, 472−478.
(36) Kim, J.; Cote, L. J.; Kim, F.; Yuan, W.; Shull, K. R.; Huang, J. X. Graphene Oxide Sheets at Interfaces. *J. Am. Chem. Soc.* **2010**, *132*, 8180−8186.
(37) Kim, J.; Cote, L. J.; Huang, J. X. Two Dimensional Soft Material: New Faces of Graphene Oxide. *Acc. Chem. Res.* **2012**, *45*, 1356−1364.
(38) Niu, Z. Q.; Liu, L. L.; Zhang, L.; Shao, Q.; Zhou, W. Y.; Chen, X. D.; Xie, S. S. A Universal Strategy to Prepare Functional Porous Graphene Hybrid Architectures. *Adv. Mater.* **2014**, *26*, 3681−3687.
(39) Shanmugasundaram, A.; Ramireddy, B.; Basak, P.; Manorama, S. V.; Srinath, S. Hierarchical $In(OH)_3$ as a Precursor to Mesoporous In_2O_3 Nanocubes: A Facile Synthesis Route, Mechanism of Self-Assembly, and Enhanced Sensing Response toward Hydrogen. *J. Phys. Chem. C* **2014**, *118*, 6909−6921.
(40) Zhu, H.; Wang, X. L.; Yang, F.; Yang, X. R. Template-Free, Surfactantless Route to Fabricate $In(OH)_3$ Monocrystalline Nano-architectures and their Conversion to In_2O_3. *Cryst. Growth Des.* **2008**, *8*, 950−956.
(41) Das, A. K.; Srivastav, M.; Layek, R. K.; Uddin, M. E.; Jung, D.; Kim, N. H.; Lee, J. H. Iodide-Mediated Room Temperature Reduction of Graphene Oxide: A Rapid Chemical Route for the Synthesis of a Bifunctional Electrocatalyst. *J. Mater. Chem. A* **2014**, *2*, 1332−1340.
(42) Shen, Y. X.; Zhang, H. B.; Zhang, H. K.; Ren, W. J.; Dasari, A.; Tang, G. S.; Yu, Z. Z. Structural Evolution of Functionalized Graphene Sheets during Solvothermal Reduction. *Carbon* **2013**, *56*, 132−138.
(43) Farvid, S. S.; Dave, N.; Radovanovic, V. P. Phase-Controlled Synthesis of Colloidal In_2O_3 Nanocrystals via Size-Structure Correlation. *Chem. Mater.* **2010**, *22*, 9−11.
(44) Huang, L.; Wang, Z. P.; Zhang, J. K.; Pu, J. L.; Lin, Y. J.; Xu, S. H.; Shen, L.; Chen, Q.; Shi, W. Z. Fully Printed, Rapid-Response Sensors Based on Chemically Modified Graphene for Detecting NO_2 at Room Temperature. *ACS Appl. Mater. Interfaces* **2014**, *6*, 7426−7433.
(45) Paul, R. K.; Badhulika, S.; Saucedo, N. M.; Mulchandani, A. Graphene Nanomesh as Highly Sensitive Chemiresistor Gas Sensor. *Anal. Chem.* **2012**, *84*, 8171−8178.
(46) Randeniya, L. K.; Shi, H.; Barnard, A. S.; Fang, J.; Martin, P. J.; Ostrikov, K. K. Harnessing the Influence of Reactive Edges and Defects of Graphene Substrates for Achieving Complete Cycle of Room-Temperature Molecular Sensing. *Small* **2013**, *9*, 3993−3999.
(47) Su, P. G.; Shieh, H. C. Flexible NO_2 Sensors Fabricated by Layer-by-Layer Covalent anchoring and in situ reduction of graphene oxide. *Sens. Actuators, B* **2014**, *190*, 865−872.
(48) Chung, M. G.; Kim, D. H.; Lee, H. M.; Kim, T.; Choi, J. H.; Seo, D. K.; Yoo, J. B.; Hong, S. H.; Kang, T. J.; Kim, Y. H. Highly Sensitive NO_2 Gas Sensor Based on Ozone Treated Graphene. *Sens. Actuators, B* **2012**, *166−167*, 172−176.
(49) Xu, P. C.; Cheng, Z. X.; Pan, Q. Y.; Xu, J. Q.; Xiang, Q.; Yu, W. J.; Chu, Y. L. High Aspect Ratio In_2O_3 Nanowires: Synthesis, Mechanism and NO_2 Gas-Sensing Properties. *Sens. Actuators, B* **2008**, *130*, 802−808.
(50) Cheng, Z. X.; Song, L. Y.; Ren, X. H.; Zheng, Q.; Xu, J. Q. Novel Lotus Root Slice-Like Self-Assembled In_2O_3 Microspheres: Synthesis and NO_2-Sensing Properties. *Sens. Actuators, B* **2013**, *176*, 258−263.